

# <sup>18</sup>F-ZW-104: A New Radioligand for Imaging Neuronal Nicotinic Acetylcholine Receptors—In Vitro Binding Properties and PET Studies in Baboons

Héric Valette<sup>1</sup>, Yingxiang Xiao<sup>2</sup>, Marie-Anne Peyronneau<sup>1</sup>, Annelaure Damont<sup>1</sup>, Alan P. Kozikowski<sup>3</sup>, Zhi-Liang Wei<sup>3</sup>, Michael Kassiou<sup>4-6</sup>, Kenneth J. Kellar<sup>2</sup>, Frédéric Dollé<sup>1</sup>, and Michel Bottlaender<sup>1</sup>

<sup>1</sup>CEA, I2BM, Service Hospitalier Frédéric Joliot, LIME, Orsay, France; <sup>2</sup>Department of Pharmacology, Georgetown University School of Medicine, Washington, DC; <sup>3</sup>Drug Discovery Program, Department of Medicinal Chemistry and Pharmacognosy, College of Pharmacy, University of Illinois at Chicago, Chicago, Illinois; <sup>4</sup>School of Chemistry, University of Sydney, Sydney, New South Wales, Australia; <sup>5</sup>Discipline of Medical Radiation Sciences, University of Sydney, Sydney, New South Wales, Australia; and <sup>6</sup>Brain and Mind Research Institute, University of Sydney, Camperdown, New South Wales, Australia

An extensive series of radioligands has been developed for imaging central nicotinic acetylcholine receptors (nAChRs) with PET. Two halogeno-derivatives of A-85380 are being used in humans. Nevertheless, these derivatives still display too-slow brain kinetics and low signal-to-noise ratio. **Methods:** A novel nAChR radioligand, 5-(6-fluorohexyn-1-yl)-3-[2(S)-2-azetidylmethoxy]pyridine (ZW-104), was characterized in vitro using competition binding assays (nAChR subtypes heterologously expressed in HEK 293 cells and in native  $\alpha 4\beta 2$  nAChRs from rat brain). <sup>18</sup>F-ZW-104 was prepared as follows: no-carrier-added nucleophilic aliphatic radiofluorination of the corresponding *N*-Boc-protected tosyloxy derivative 5-(6-tosyloxyhexyn-1-yl)-3-[2(S)-(N-(tert-butoxycarbonyl))-2-azetidylmethoxy]pyridine with the activated 4,7,13,16,21,24-hexaoxa-1,10-diazabicyclo-[8,8,8]hexacosane (K-<sup>18</sup>F-F-Kryptofix 222 [K<sub>222</sub>] complex), followed by quantitative trifluoroacetic acid-induced removal of the *N*-Boc protective group. <sup>18</sup>F-ZW-104 was then studied in baboons using PET. **Results:** ZW-104 showed high binding affinities for rat  $\alpha 4\beta 2$  nAChRs (K<sub>i</sub>, 0.2 nM) and other subtypes containing the  $\beta 2$  subunit but much lower affinities for rat  $\alpha 3\beta 4$  nAChRs (K<sub>i</sub>, 5,500 nM) and other subtypes containing the  $\beta 4$  subunit. The regional radioactivity distribution in the baboon brain matched that of the  $\alpha 4\beta 2$  nAChR, which was similar to that of 2-<sup>18</sup>F-fluoro-3-(2(S)-azetidylmethoxy)pyridine (2-<sup>18</sup>F-A-85380), a radioligand used in humans. Comparison between <sup>18</sup>F-ZW-104 and 2-<sup>18</sup>F-A-85380 demonstrated better in vivo binding properties of the new radioligand: a substantially greater amount of radioactivity accumulated in the brain, and the occurrence of peak uptake in the thalamus was earlier than that of 2-<sup>18</sup>F-A-85380 and was followed by washout. Distribution volume values in different brain regions were 2-fold higher for <sup>18</sup>F-ZW-104 than for 2-<sup>18</sup>F-A-85380. Displacement by nicotine or unlabeled ZW-104 demonstrated a lower nonspecific binding than that of 2-F-A-85380.

**Conclusion:** These results suggest that <sup>18</sup>F-ZW-104 is a promising PET radioligand for studying nAChRs containing the  $\beta 2$  subunits in humans.

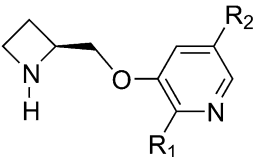
**Key Words:** positron emission tomography; central nicotinic receptors; in vitro binding;  $\beta 2$  subunit

**J Nucl Med 2009; 50:1349–1355**  
DOI: 10.2967/jnumed.108.061374

A loss of cholinergic neurons has been associated with several pathologic disorders (1), such as dementia of the Alzheimer type and Parkinson disease. PET offers the opportunity to monitor changes in human nicotinic acetylcholine receptors (nAChRs) in vivo. However, there are certain difficulties in the development of suitable radioligands for the in vivo imaging of nAChRs (2), one of them being the low density of nAChRs in extrathalamic areas. Therefore, there is a need for radioligands with high affinities (probably less than 1 nM) and radiosyntheses yielding high specific radioactivities. The role of lipophilicity of the radioligand remains a subject of debate, but a relationship exists between the lipophilicity and non-displaceable binding. Research efforts from radiochemists have focused on the development of highly specific radioligands with improved brain kinetics (2). A new emerging, promising field is the use of antagonists at nAChRs (3,4), but these compounds need more experiments to confirm their preliminary attractive characteristics.

The agonists 2-fluoro- and 5-iodo-A-85380 (Fig. 1, compounds 1 and 2) are the only PET/SPECT radioligands used in humans today. However, these agonists have 3 drawbacks: slow kinetics, low signal-to-noise ratio, and a large amount of nondisplaceable binding. The presence of a bulky halogen (an iodine) at the 5-position of the pyridinyl

Received Dec. 16, 2008; revision accepted Apr. 8, 2009.  
For correspondence or reprints contact: Héric Valette, Service Hospitalier Frédéric Joliot, CEA, I2BM/LIME, F-91401 Orsay, France.  
E-mail: heric.valette@cea.fr  
COPYRIGHT © 2009 by the Society of Nuclear Medicine, Inc.



Cpd		R <sub>1</sub>	R <sub>2</sub>
1	2- <sup>18</sup> F-A-85380	<sup>18</sup> F	H
2	5- <sup>123</sup> I-A-85380	H	<sup>123</sup> I
3	sazetidine	H	C≡C(CH <sub>2</sub> ) <sub>4</sub> OH
4	<sup>18</sup> F-ZW-104	H	C≡C(CH <sub>2</sub> ) <sub>4</sub> <sup>18</sup> F

**FIGURE 1.** Chemical structures of 2-<sup>18</sup>F-A-85380, 5-<sup>123</sup>I-A-85380, sazetidine, and <sup>18</sup>F-ZW-104.

ring in 5-iodo-A-85380 does not affect the affinity for nAChRs but leads to an increase of selectivity for  $\alpha 4\beta 2$  subtype (5–8). Therefore, recently derivatives of azetidines A-85380 (and also pyrrolidine A-84543, structure not shown) bearing a 5-alkynyl substituent were reported (9), following the idea that a more bulky substituent such as an 5-alkynyl would not decrease but perhaps increase the affinity and selectivity of the compounds at  $\alpha 4\beta 2$  nAChRs. Within this series, we have been interested in the pharmacologic properties of 5-(6-hydroxyhexyn-1-yl)-3-[2(S)-2-azetidylmethoxy]pyridine (Fig. 1, compound 3), which is a selective nAChR agonist (10). This compound is a derivative of A-85380 (11), which itself has high affinity and selectivity for nAChRs containing  $\beta 2$  subunits (12). 5-(6-fluorohexyn-1-yl)-3-[2(S)-2-azetidylmethoxy]pyridine (ZW-104; Fig. 1, compound 4) is structurally closely related to 5-(6-hydroxyhexyn-1-yl)-3-[2(S)-2-azetidylmethoxy]pyridine, with the terminal hydroxyl group replaced by a fluorine atom.

In this study, we characterized the *in vitro* binding affinity and selectivity of ZW-104. We also labeled ZW-104 with <sup>18</sup>F and investigated in rats and baboons the *in vivo* properties of this novel radioligand to selectively image central  $\alpha 4\beta 2$  nAChRs.

## MATERIALS AND METHODS

### Radiochemistry

**Chemicals.** Chemicals were purchased from Aldrich, Fluka, or Sigma France and were used without further purification. ZW-104 (as reference compound) and the corresponding *N*-Boc-protected tosyloxy derivative 5-(6-tosyloxyhexyn-1-yl)-3-[2(S)-(*N*-(tert-butoxycarbonyl))-2-azetidylmethoxy]pyridine (as precursor for labeling with <sup>18</sup>F) were synthesized according to literature procedures (9).

**High-Performance Liquid Chromatography (HPLC) Analyses.** For HPLC method A, the system was equipped with a Waters 600 pump and Waters 600 controller, a Shimadzu SPD10-AVP ultraviolet (UV)-multiwavelength detector, and a miniature ionisation chamber probe. The column was a semipreparative Zorbax C18

(Hewlett-Packard; 250 × 9.4 mm), porosity was 5  $\mu$ m, the eluent was 0.9% aqueous NaCl/EtOH/AcOH:800/200/1 (v/v/v), flow rate was 6 mL/min, and absorbance detection was at  $\lambda = 254$  nm. Room temperature was used. For HPLC method B, the system was equipped with a Waters Alliance 2690 (or a Waters binary HPLC pump 1525) with a UV spectrophotometer (Photodiode Array Detector; Waters 996) and a Berthold LB509 radioactivity detector. The column was an analytic Symmetry-M C18 (Waters; 50 × 4.6 mm); porosity was 5.0  $\mu$ m; the conditions were isocratic elution with solvent A/solvent B:63/37 (v/v) (solvent A, H<sub>2</sub>O containing low-UV PIC B7 reagent [Waters; 20 mL for 1,000 mL] and solvent B, H<sub>2</sub>O/CH<sub>3</sub>CN:30/70 (v/v) containing low-UV PIC B7 reagent [Waters; 20 mL for 1,000 mL]). The flow rate was 2.0 mL/min, and absorbance detection was at  $\lambda = 254$  nm. Room temperature was used.

**Miscellaneous.** Radiosyntheses using <sup>18</sup>F, including the HPLC purifications, were performed in a 7.5-cm lead-shielded cell using a computer-assisted Zymate-XP robot system (Zymark Corp.).

**Radioisotope Production.** No-carrier-added aqueous <sup>18</sup>F-fluoride ion was produced via the <sup>18</sup>O(p, n)<sup>18</sup>F nuclear reaction by irradiation of 2 mL of <sup>18</sup>O-water (>97%-enriched; CortecNet) target on an IBA Cyclone-18/9 cyclotron (18-MeV proton beam) and was transferred to the appropriate hot cell.

**Preparation of 4,7,13,16,21,24-hexaoxa-1,10-diazabicyclo[8.8.8]-hexacosane (*K*-<sup>18</sup>F-F-Kryptofix 222 [*K*<sub>222</sub>], Complex.** <sup>18</sup>F (half-life, 109.8 min) as <sup>18</sup>F-fluoride ion was isolated by passing the irradiated <sup>18</sup>O-water target, using helium pressure (1.5–2.0 bar), through an anion-exchange resin (Sep-pak Light Accell Plus QMA; Waters) cartridge (chloride form, washed beforehand with aqueous 1 M NaHCO<sub>3</sub> (2 mL) and rinsed with water (20 mL) and CH<sub>3</sub>CN (10 mL)). Helium was blown through the column to maximally extract <sup>18</sup>O-water. The <sup>18</sup>F-fluoride ion was then eluted from the resin, using an aqueous K<sub>2</sub>CO<sub>3</sub> solution (1.0 mL of a 4.5-mg solution per milliliter), into a Vacutainer tube (Becton, Dickinson) containing *K*-<sup>18</sup>F-F-K<sub>222</sub> (12.0–15.0 mg; Fluka). The resulting solution was then gently concentrated to dryness at 145°C–150°C under a nitrogen stream for 10 min to give no-carrier-added *K*-<sup>18</sup>F-F-K<sub>222</sub> complex as a white semisolid residue.

**Preparation of <sup>18</sup>F-ZW-104.** For radiosynthesis, acetonitrile (600  $\mu$ L) containing 5-(6-tosyloxyhexyn-1-yl)-3-[2(S)-(*N*-(tert-butoxycarbonyl))-2-azetidylmethoxy]pyridine (6–10 mg) was added into the Vacutainer tube containing the dried *K*-<sup>18</sup>F-F-K<sub>222</sub> complex. The nonsealed tube was thoroughly stirred in a vortex mixer (30 s) and then placed in a heating block (at 120°C, for 8 min) without stirring the contents. The reaction vessel was then cooled using an ice-water bath; the reaction mixture was diluted with water (1 mL) and transferred onto a C18 cartridge (PrepSep R-C18 Extraction Column; Fisher Scientific), prefilled with water (2 mL). The tube was rinsed twice with water (1 mL), which was also transferred and added to the diluted reaction mixture on top of the cartridge. An additional portion of water (2 mL) was further added to the diluted reaction mixture on top of the cartridge. The entire contents were then passed through the cartridge, which was then washed with water (3 mL) and partially dried for 0.5 min by applying a nitrogen stream. *N*-Boc-protected <sup>18</sup>F-ZW-104 was eluted from the cartridge with CH<sub>2</sub>Cl<sub>2</sub> (3 mL) into a 5-mL reaction vial containing trifluoroacetic acid (TFA) (0.1 mL). Elution was repeated twice with 1 mL of CH<sub>2</sub>Cl<sub>2</sub> for maximal transfer of the <sup>18</sup>F-labeled intermediate. The resulting CH<sub>2</sub>Cl<sub>2</sub>/TFA solution (50/1, v/v) was then concentrated to dryness at 65°C–75°C under a gentle nitrogen stream for 3–5 min. The

residue was redissolved in  $\text{CH}_2\text{Cl}_2$  (2 mL) and concentrated again to dryness to minimize TFA presence (at  $65^\circ\text{C}$ – $75^\circ\text{C}$  under a gentle nitrogen stream for 2–3 min). Finally, the residue was redissolved in the HPLC solvent used for purification (1.0 mL), and the crude was injected onto HPLC (HPLC method A). Isocratic elution gave pure  $^{18}\text{F}$ -ZW-104 (retention time [ $t_{\text{R}}$ ], 17.0–18.0 min). For quality control, final chemical identification of  $^{18}\text{F}$ -ZW-104 was performed on an aliquot of the HPLC-collected fraction by analytic HPLC (HPLC method B), with a sample of authentic ZW-104 ( $t_{\text{R}}$ , 2.34 min). Chemical and radiochemical purities were also assessed on this aliquot by HPLC (HPLC method B). Specific radioactivity of the radioligand was calculated from 3 consecutive HPLC analyses and determined as follows: the area of the UV absorbance peak corresponding to the radiolabeled product was measured (integrated) on the HPLC chromatogram and compared with a standard curve relating mass to UV absorbance. The specific radioactivity follows from the found mass and the associated collected radioactivity.

### In Vitro Pharmacology

**Stably Transfected Cell Lines and Cell Culture.** Stably transfected cell lines expressing defined rat nAChR subtypes were described previously (6,13). Tissue culture medium and antibiotics were obtained from Invitrogen Corp. Fetal bovine serum was provided by Gemini Bio-Products. Cells were grown at  $37^\circ\text{C}$  with 5%  $\text{CO}_2$  in a humidified incubator.

**Radioligand Binding Assay.** Competition binding assays using  $^3\text{H}$ -epibatidine have been described previously (13). In brief, cultured cells at greater than 80% confluence were removed from their flasks and placed in 10 mL of 50 mM Tris-HCl buffer (pH 7.4,  $4^\circ\text{C}$ ). The cell suspension was centrifuged at  $10,000g$  for 5 min, and the pellet was collected. The cell pellet was then homogenized in 10 mL of buffer with a Polytron homogenizer (12-mm aggregate, 26,000 rpm, 20 s; model PT2100; Kinematica) and centrifuged at  $36,000g$  for 10 min at  $4^\circ\text{C}$ . The membrane pellet was resuspended in fresh buffer, and aliquots of the membrane preparation equivalent to 30–200  $\mu\text{g}$  of protein were used for binding assays. The concentration of  $^3\text{H}$ -epibatidine used was 100 pM for competition binding. The concentrations of ZW-104 ranged from 0.1 nM to 10  $\mu\text{M}$ . The nonspecific binding was assessed in parallel incubations in the presence of 300  $\mu\text{M}$  nicotine. Bound and free ligands were separated by vacuum filtration through Whatman GF/C filters (Brandel Inc.) treated with 0.5% polyethylenimine. The filter-retained radioactivity was measured by liquid scintillation counting. The  $K_i$  (inhibition constant) values for  $^3\text{H}$ -epibatidine used for calculating  $K_i$  values (nanomoles) were 0.02 for  $\alpha 4\beta 2$ , 0.08 for  $\alpha 2\beta 4$ , 0.03 for  $\alpha 3\beta 2$ , 0.3 for  $\alpha 3\beta 4$ , 0.04 for  $\alpha 4\beta 2$ , 0.09 for  $\alpha 4\beta 4$ , and 0.05 for rat forebrain. Data from saturation and competition binding assays were analyzed using Prism 4 (GraphPad Software).

### Determination of Plasma and Brain Metabolites in Rats

Before testing the radioligand in baboons, plasma and brain metabolites were assessed in rats. Four male Sprague–Dawley rats (weight, 250 g) were infused through a tail vein with  $^{18}\text{F}$ -ZW-104 ( $32.5 \pm 12.2$  MBq) and sacrificed 30 or 70 min later, with blood (1 mL) collected at each time point. The brain was excised and homogenized in 4 mL of  $\text{CH}_3\text{CN}$ . Plasma (500  $\mu\text{L}$ ) was deproteinized (with 700  $\mu\text{L}$  of  $\text{CH}_3\text{CN}$ ) and injected onto the HPLC column for the determination of percentage of unchanged  $^{18}\text{F}$ -

ZW-104. The activity of brain homogenates was counted with the  $\gamma$ -counter, and the samples were centrifuged at  $3,500g$  for 2 min at  $4^\circ\text{C}$ . The supernatants then were injected onto the HPLC column. The HPLC system included a P680A gradient quaternary pump, an ASI100T auto sampler, a UVD170U UV-VIS detector (Summit Performance), and a LB507 radioisotope detector (MXZ 500-4 cell, Berthold). The eluents consisted of 0.1% TFA in water (solution A) and 0.1% TFA in acetonitrile (solution B).  $^{18}\text{F}$ -ZW-104 and its radiolabeled metabolites were separated at room temperature on a C18  $\mu$ Bondapak semipreparative column ( $300 \times 7.8$  mm, 10  $\mu\text{m}$ ; Waters). The column was equilibrated with 80% of solution A and 20% of solution B, and a linear gradient from 20% to 30% solution B was applied for 10 min. The flow rate was 4 mL/min (UV detection, 220 nm). Data acquisition and processing were performed using Chromeleon software (version 5.0; Dionex). The radioactivity due to unchanged  $^{18}\text{F}$ -ZW-104 was expressed as a fraction of the total radioactive peak areas.

### In Vivo PET in Baboons

**Animals.** All animal-use procedures were in strict accordance with the recommendations of the European Community (86/609/CEE) and the French National Committee (décret 87/848) for the care and use of laboratory animals.

**MRI.** For each baboon, MR images were obtained in a separate experiment (1.5-T Signa; GE Healthcare). A T1-weighted inversion-recovery sequence in 3-dimensional mode and a  $256 \times 192$  matrix over 124 slices (1.5-mm thick) were used to generate the MR images compatible with the PET images.

**PET.** PET studies of the brain distribution of radiolabeled compound were performed in adult *Papio anubis* baboons. Two hours before the PET acquisition, the animals received ketamine (10 mg/kg intramuscularly). After being intubated, animals were artificially ventilated and anesthetized with 66%  $\text{N}_2\text{O}$  and 1% isoflurane (OAV 7710; Ohmeda). PET experiments were performed with an HR+ Exact positron tomograph (CTI PET Systems). This scanner allowed the simultaneous acquisition of 63 slices every 2.2 mm, with spatial and axial resolutions of 4.5 mm. Transmission scans were acquired for 15 min using 3 retractable  $^{68}\text{Ge}$  rod sources. The baboon's head was positioned in the tomograph using a custom-designed stereotactic head holder. Five baboons (mean weight  $\pm$  SD,  $12.6 \pm 4.3$  kg) underwent a total of 8 PET experiments. They were injected intravenously with  $^{18}\text{F}$ -ZW-104 ( $152 \pm 37$  MBq;  $6.3 \pm 1.2$  nmol) and imaged for at least 180 min. During PET acquisition, arterial blood samples were withdrawn from the femoral artery at designated times. To better define the kinetics of the radioligand, the duration of 2 PET experiments was extended to 6 h. In 1 baboon after brain imaging, a whole-body scan (180 min after injection of the radioligand) of  $^{18}\text{F}$ -ZW-104 distribution was obtained (5 steps; duration of each step, 7 min), followed by a segmented transmission. We examined whether the cerebral uptake of the radioligand could be displaced ( $n = 2$ ) by injecting, 120 min after the beginning of the PET experiment, either nicotine (2,500 nmol/kg intravenously,  $n = 1$ ) or unlabeled ZW-104 (500 nmol/kg intravenously,  $n = 1$ ). PET was continued for an additional 120 min. In 1 experiment, displacement by nicotine (bolus, 1,850 nmol/kg, followed by an infusion of 1,850 nmol/kg over 3 h) was scanned for 4 h. Heart rate, end tidal  $\text{pCO}_2$ , and rectal temperature were continuously monitored during all the PET experiments. Two presaturation experiments were performed using either unlabeled ZW-104 (500 nmol/kg) injected as a slow bolus (10 min) 50 min

before injection of the radioligand or nicotine (2,500 nmol/kg) administered 30 min before the radioligand. These PET experiments lasted for 180 min. For comparison of the uptake and brain kinetics of the 2 radioligands, 1 baboon was intravenously injected with 74 MBq (2 mCi (1 nmol)) of 2-<sup>18</sup>F-A-85380 and imaged for 3 h.

**PET Data Analysis.** For PET data analysis, regions of interest were delineated on images on which anatomic structures (frontal cortex, thalamus, striata, and cerebellum) can be clearly identified. The position of the volumes of interest (VOI) was controlled on the MR images. On the basis of clearly identified anatomic structures, 9 VOIs were delineated in 3 dimensions on T1-weighted MR images: frontal, parietal, and temporal and occipital cortices; caudate nucleus; putamen; thalamus; cerebellum; and hippocampus. Coregistration of PET images to the corresponding MR images was used to ensure the consistency of the anatomic localization of <sup>18</sup>F-ZW-104 cerebral binding. To generate each regional time–activity curve, the mean radioactivity in the VOI was calculated for each frame, corrected for <sup>18</sup>F decay, plotted versus time, and expressed as standardized uptake value (SUV) (i.e., [MBq/mL of tissue]/injected dose [MBq]/body weight [g]). After a displacement experiment, the percentage changes in thalamic and cerebellar radioactivities were calculated at the end of the PET experiment (240 min) by dividing the difference in radioactivity (control experiment – challenge experiment) by the value of the radioactivity in the control experiment at 240 min.

The Logan graphical (14) analysis of reversible radioligand kinetics was applied to the present data. This method allows for the measurement of the total distribution volume ( $V_T$ ) of the ligand without any assumption on the actual configuration of the tissue compartments.  $V_T$  was computed by linear regression of the final part of the plot using PMOD software (PMOD Group; <http://www.pmod.com>).

**Determination of Plasma Metabolites in Baboons.** Arterial blood samples (3 mL) were collected at 5, 10, 20, 30, 60, 90, 120, and 160 min after the injection of the tracer and immediately centrifuged (5 min, 2,000g, at 4°C) to obtain cell-free plasma. For deproteinization, 0.5 mL of plasma was mixed with 0.7 mL of acetonitrile. After centrifugation at 3,500g for 5 min, the supernatant (about 1.1 mL) was directly injected onto the HPLC column.

## RESULTS

Data are presented as mean ± SD.

## Chemistry

ZW-104 was labeled with <sup>18</sup>F using the following non-optimized 2-step radiochemical process: no-carrier-added nucleophilic aliphatic radiofluorination of the corresponding *N*-Boc-protected tosyloxy derivative (6 mg) with the activated K-<sup>18</sup>F-F-K<sub>222</sub> complex in acetonitrile at 120°C for 8 min, followed by quantitative TFA-induced removal of the *N*-Boc protective group and finally semipreparative HPLC purification on a Zorbax C18 column (Hewlett-Packard) using a mixture of solvents directly compatible with an intravenous injection (0.9% aqueous NaCl/EtOH/AcOH:800/200/1 [v/v/v]). Typically, 1.11–1.85 GBq of radiochemically pure (>99%) <sup>18</sup>F-ZW-104 (37–74 GBq/μmol) could be obtained within 100 min, starting from 37.0 GBq of <sup>18</sup>F-fluoride.

## Binding Affinities of ZW-104 for nAChR Subtypes

ZW-104 bound with high affinities to rat α4β2, α3β2, and α2β2 nAChR subtypes heterologously expressed in HEK 293 cells and to native α4β2 nAChRs from rat brain (Table 1). The binding affinity of ZW-104 for α4β2 receptors is 28,000 times higher than that for α3β4 receptors. The selectivity of ZW-104 for α4β2 receptors over α3β4 receptors was much greater than that of 5-iodo-A-85380 ( $K_i$  ratio, 4,700) or 2-F-A-85380 ( $K_i$  ratio, 2,700), both of which are considered as relatively selective ligands for α4β2 nAChRs. ZW-104 also binds to α2β2 and α3β2 subtypes with high affinities, though they are slightly lower than that to α4β2 subtype. Therefore, ZW-104 appears to be selective for the β2 containing nAChRs.

## Metabolites in Rat Plasma and Brain

Plasma HPLC analysis showed that unchanged <sup>18</sup>F-ZW-104 represented 38% ± 9% and 17.5% ± 2.3% at 30 and 70 min after injection, respectively. In the brain, only authentic <sup>18</sup>F-ZW-104 could be detected until 70 min after injection.

## PET Studies in Baboons

Brain kinetics in control animals are presented in Figure 2. As expected, the thalamus had the higher uptake (maximum standardized uptake value [SUV<sub>max</sub>] 5.72 at 35–50 min after injection), followed by a slow washout (3.49 at

**TABLE 1.** Inhibition Constants ( $K_i$ , nM) at nAChR Subtypes of Nicotinic Reference Ligands and of PET SPECT Radioligands

Ligand	$K_i$ (nmoles)						Rat forebrain
	α2β2	α2β4	α3β2	α3β4	α4β2	α4β4	
ZW-104	0.8	200	0.64	5,500	0.2	120	0.36
5-iodo-A-85380	0.031	41	0.47	280	0.059	24	0.11
2-fluoro-A-85380	1.44	181	3.02	3,680	1.33	188	0.47
Iodo-epibatidine	0.11	0.15	0.18	0.98	0.15	0.15	0.33
(–)-Nicotine	12	110	47	440	10	40	12

Inhibition constants of ligands at 6 defined rat nAChR subtypes and native nAChRs in rat forebrain (mainly α4β2 subtype) were measured. nAChRs were labeled with <sup>3</sup>H-epibatidine. For comparison, data published previously are shown here, including  $K_i$  values of 5-iodo-A-85380, 2-fluoro-A-85380, Iodo-epibatidine, and (–)-nicotine (4,6).



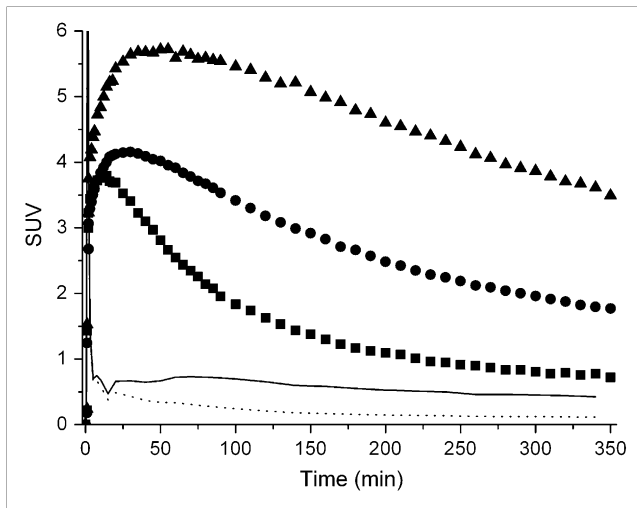


**FIGURE 2.** Baboon brain time-activity curves (SUV) after intravenous injection of  $^{18}\text{F}$ -ZW-104. Peak radioactivity in thalamus ( $\blacktriangle$ ) occurred at 50–60 min and was followed by clear washout. In regions with low nAChR densities, frontal cortex ( $\bullet$ ) and cerebellum ( $\blacksquare$ ) washout was faster. Plasma (continuous line) and plasma-unchanged ZW-104 (dotted line) radioactivities are also displayed.

350 min after injection). Caudate nucleus, putamen, and cortices had an intermediate uptake, whereas the cerebellum showed the lowest uptake (2.80 SUV<sub>max</sub> at 35 min after injection) and the fastest washout (0.71 SUV at 350 min after injection). The radioactivity ratio for thalamus to cerebellum increased with time until 230 min and remained stable at a value of 4.6–4.8 until 360 min. Logan analysis demonstrated that 30, 45, and 55 min are required for  $V_T$  to become time-invariant in the cerebellum, frontal cortex, and thalamus, respectively (Fig. 3). Ratio of thalamic  $V_T$  to cerebellar  $V_T$  (Logan plot) was 3.5 at 180 min and remained unchanged at 360 min after injection. For comparison, this ratio was 2.38 at 180 min after injection with 2-F-A-85380. Pretreatment with nicotine reduced uptake in the thalamus to 2.80 SUV at 35 min (Fig. 4). Pretreatment with ZW-104 reduced uptake in the thalamus to 3.05 SUV<sub>max</sub> at 35 min, and it was followed by a steep washout (Fig. 4). At 180 min after injection, uptake in the thalamus was drastically reduced 1.23 and 117 SUV after nicotine or ZW-104 before treatment, respectively; Fig. 4). These reductions represented a saturation of the radioligand uptake by 80% and 75%, respectively.

Injection of unlabeled ZW-104 produced a steep washout ( $t_{1/2}$ , 65 min). Radioactivity in the thalamus decreased from 4.18 SUV (just before the displacement) to 1.23 in 2 h. Radioactivity in the cerebellum decreased from SUV 1.53 to 0.74. Injection of nicotine produced a washout ( $t_{1/2}$  = 67 min). Radioactivity in the thalamus decreased from 5.63 SUV (just before the displacement) to 1.76 SUV in 4 h. Radioactivity in the cerebellum decreased from 2.19 to 1.06 SUV. Therefore, when these results are compared with the

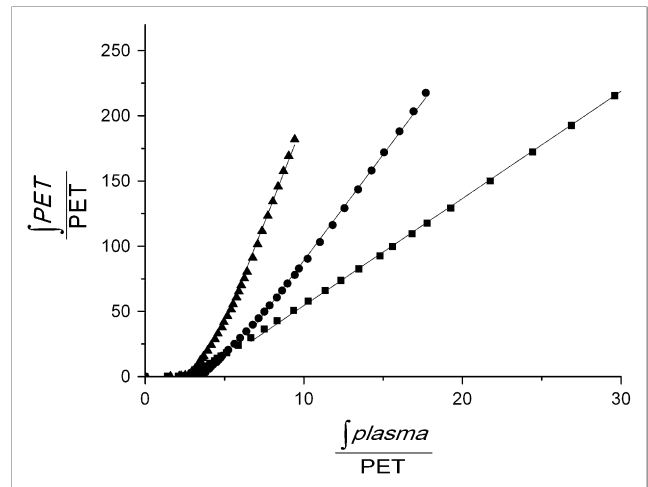


**FIGURE 3.** Logan plots in thalamus, frontal cortex, and cerebellum. For  $V_T$  to be time-invariant in cerebellum, frontal cortex, and thalamus, 30, 45, and 55 min, respectively, are required.

6-h control experiment, the percentage of displaceable binding could be estimated at 83% with nicotine and at 80% with ZW-104.

The whole-body images (obtained 185 min after injection of  $^{18}\text{F}$ -ZW-104; Fig. 5) showed a high accumulation of radioactivity in the kidney and bladder and in the gallbladder and intestine, suggesting 2 main routes of elimination through the renal and the hepatobiliary systems. Uptake in the bone was low.

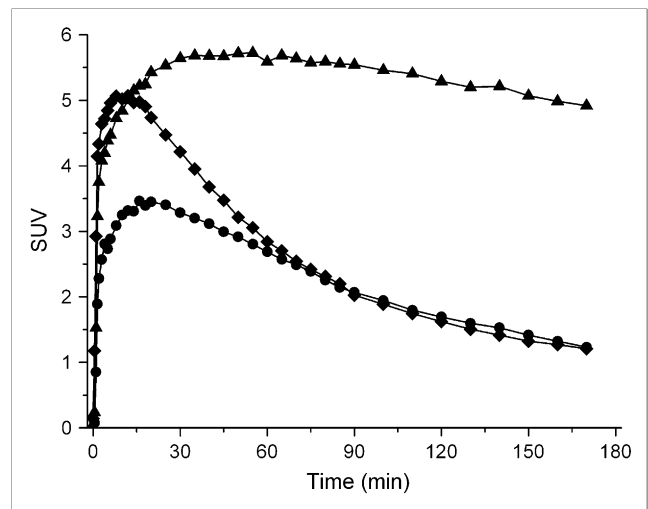


**FIGURE 4.** Thalamic time-activity curves in control animal ( $\blacktriangle$ ) and after pretreatment with intravenous nicotine ( $\bullet$ ), 2,500 nmol/kg administered 30 min before the radiotracer, or unlabeled ZW-104 ( $\blacklozenge$ ), 500 nmol/kg administered 50 min before the radiotracer.

**FIGURE 5.** Whole-body distribution of  $^{18}\text{F}$ -ZW-104. Projection obtained 3 h after injection. Elimination of radioligand through biliary system and kidneys.

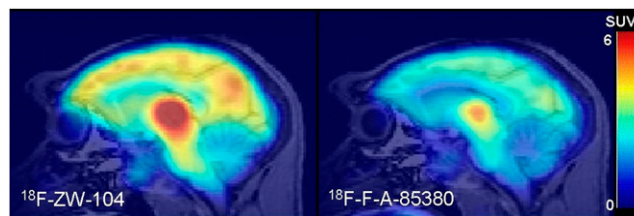
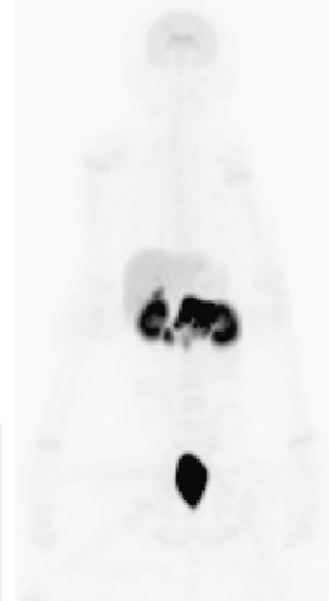


**FIGURE 6.** Sagittal sum images (from 45 to 90 min) after injection of  $^{18}\text{F}$ -ZW-104 and  $2\text{-}^{18}\text{F}$ -A-85380.

### Plasma Metabolites in Baboons

Unchanged fraction of  $^{18}\text{F}$ -ZW-104 in baboon ( $n = 3$ ) plasma at 30, 50, and 120 min represented  $64\% \pm 5\%$ ,  $50\% \pm 8\%$ , and  $32\% \pm 12\%$ , respectively, of total radioactivity. The  $t_R$  of ZW-104, in the present experimental conditions, was 8.2 min. At 90 min after injection, 5 labeled metabolites were detected: 4 had shorter  $t_R$  (1.3, 3.33, 4.67, and 6.83 min), and 1  $t_R$  was longer (9.5 min). This latter accounted for 7% of the radioactivity at 160 min after injection, and unchanged  $^{18}\text{F}$ -ZW-104 represented 27% of plasma radioactivity. The HPLC profile of ZW-104 was obtained in acidic conditions, and therefore no conclusions about the lipophilicity of the radioactive metabolites at physiologic pH can be made from these data.

### DISCUSSION

The present study shows that ZW-104 has a high binding affinity for the  $\alpha 4\beta 2$  nAChR subtype. Although it has slightly lower affinities for the heterologously expressed  $\alpha 4\beta 2$  subtype and native  $\alpha 4\beta 2$  receptors from rat forebrain than those of 5-iodo-A-85380, binding affinities of ZW-104 for this receptor subtype are higher than those of 2-F-A-85380 (Table 1). ZW-104 displays better selectivity for  $\alpha 4\beta 2$  receptors over the  $\alpha 3\beta 4$  receptors than do 5-iodo-A-85380 and 2-F-A-85380, which indicates that ZW-104 is less likely to cause side effects mediated by  $\alpha 3\beta 4$  receptors of the autonomic nervous system.

The present PET results demonstrate that, compared with 2-F-A-85380, ZW-104 exhibits some superior properties for in vivo imaging. The regional distributions of radioactivity in *Papio anubis* brain after a bolus administration of both radioligands are notably similar and correspond to the distribution and regional densities of nAChRs in this species (Fig. 6). The contrast between nAChR-rich and -poor regions is higher with  $^{18}\text{F}$ -ZW-104. ZW-104 SUVmax

was higher than 2-F-A-85380 SUVmax (5.72 vs. 2.8). This value of SUVmax is in the same range of that observed with the nAChR antagonist (-)-7-methyl-2-*exo*-[3'-(6-[ $^{18}\text{F}$ ]fluoropyridin-2-yl)-5'-pyridinyl]-7-azabicyclo[2.2.1]heptane (4). But, with this latter the maximal accumulated radioactivity was reached earlier (7–28 min,  $n = 2$ , but the anesthesia was performed using propofol).  $V_T$  values for  $^{18}\text{F}$ -ZW-104 were roughly 2-fold higher than for  $2\text{-}^{18}\text{F}$ -A-85380 (thalamus, +132%; frontal cortex, +91%; cerebellum, +63%); brain and dissociation kinetics for  $^{18}\text{F}$ -ZW-104 were also faster than those of  $2\text{-}^{18}\text{F}$ -A-85380 (Fig. 7). The rate of  $^{18}\text{F}$ -ZW-104 metabolism in plasma after intravenous injection is similar to that of  $2\text{-}^{18}\text{F}$ -A-85380, and no metabolites were detected in the rat brain.

However,  $^{18}\text{F}$ -ZW-104 may not be the best choice for imaging areas with high concentrations of nAChRs such as the thalamus because the PET emission scan would be rather long (at least 40–50 min are needed to reach the SUVmax). Although the toxicity of ZW-104 was not addressed in the present article, the low affinity for  $\alpha 3\beta 4$  nAChRs and the high dose administered during the displacement experiment suggest a rather good safety. The following are drawbacks of  $^{18}\text{F}$ -ZW-104: it has a radiosynthesis with a lower specific radioactivity than that of  $2\text{-}^{18}\text{F}$ -A-85380. Average specific

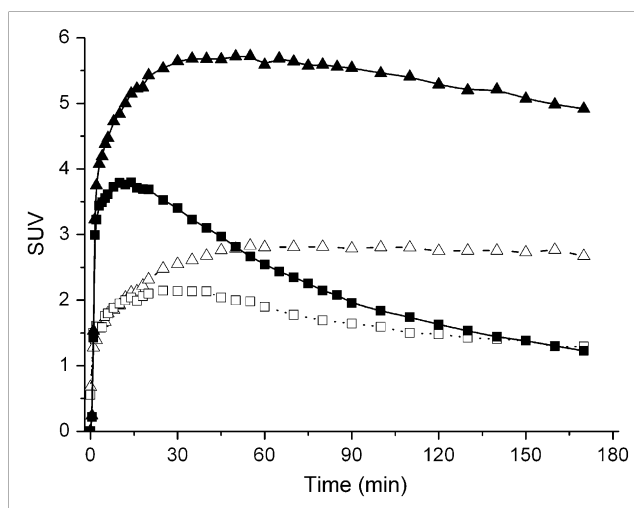


**FIGURE 7.** SUV curves of  $^{18}\text{F}$ -ZW-104 (filled symbols) and  $2\text{-}^{18}\text{F}$ -A-85380 (open symbols) in thalamus (▲) and in cerebellum (■).

radioactivity values were  $675 \pm 226$  mCi/ $\mu$ mol ( $25.0 \pm 8.4$  Bq/ $\mu$ mol) for  $^{18}\text{F}$ -ZW-104, and for 2- $^{18}\text{F}$ -A-85380 the corresponding values were  $3,128 \pm 1,314$  mCi/ $\mu$ mol ( $115.7 \pm 48.6$  GBq/ $\mu$ mol) ( $n = 34$ ; H. Valette, unpublished data, 2007–2008). Therefore, the radiosynthesis has to be optimized. We did not directly study the dose effect of  $^{18}\text{F}$ -ZW-104 on the  $V_T$  values, but, for example, a baboon injected with 0.3 nmol/kg had the same  $V_T$  value (31.5 vs. 32) as a baboon injected with 0.71 nmol/kg.  $^{18}\text{F}$ -ZW-104 has non-negligible affinity for  $\alpha_3\beta_2$  and for  $\alpha_2\beta_2$  nAChR subtypes, albeit the density of  $\alpha_3\beta_2$  and of  $\alpha_2\beta_2$  nAChRs is low in the baboon brain when compared with that of  $\alpha_4\beta_2$ : they represent only 20% of the nAChRs containing the  $\beta_2$  subunit in the striata and frontal cortex (15).

## CONCLUSION

These properties suggest that ZW-104 has potential as a radioligand for the in vivo imaging of nAChRs containing the  $\beta_2$  subunit because it demonstrated faster and higher brain uptake and higher specific binding than 2-fluoro-A-85380. This work should be further confirmed by in vivo studies using a multiinjection protocol and a compartmental analysis to determine a clear superiority over 2-fluoro-A-85380, in particular the importance of the nonspecific binding.

## ACKNOWLEDGMENTS

We thank Françoise Hinnen, Sandrine Bourgeois, and Sébastien Goutal for their technical assistance.

## REFERENCES

- Singh A, Potter A, Newhouse P. Nicotinic acetylcholine receptor system and neuropsychiatric disorders. *IDrugs*. 2004;7:1096–1103.
- Horti AG, Villemagne VL. The quest for Eldorado: development of radioligands for in vivo imaging of nicotinic acetylcholine receptors in human brain. *Curr Pharm Des*. 2006;12:3877–3900.
- Gao Y, Horti AG, Kuwabara H, et al. New synthesis and evaluation of enantiomers of 7-methyl-2-exo-(3'-iodo-5'-pyridinyl)-7-azabicyclo[2.2.1]heptane as stereoselective ligands for PET imaging of nicotinic acetylcholine receptors. *Bioorg Med Chem Lett*. 2008;18:6168–6170.
- Gao Y, Kuwabara H, Spivak CE, et al. Discovery of (–)-7-methyl-2-exo-[3'-(6-[ $^{18}\text{F}$ ]fluoropyridin-2-yl)-5'-pyridinyl]-7-azabicyclo[2.2.1]heptane, a radiolabeled antagonist for cerebral nicotinic acetylcholine receptor ( $\alpha_4\beta_2$ -nAChR) with optimal positron emission tomography imaging properties. *J Med Chem*. 2008;51:4751–4764.
- Mukhin AG, Gundisch D, Horti AG, et al. 5-Iodo-A-85380, an  $\alpha$ -4- $\beta$ -2 subtype-selective ligand for nicotinic acetylcholine receptors. *Mol Pharmacol*. 2000;57:642–649.
- Xiao Y, Kellar KJ. The comparative pharmacology and up-regulation of rat neuronal nicotinic receptor subtype binding sites stably expressed in transfected mammalian cells. *J Pharmacol Exp Ther*. 2004;310:98–107.
- Mogg AJ, Jones FA, Pullar IA, Sharples CG, Wonnacott S. Functional responses and subunit composition of presynaptic nicotinic receptor subtypes explored using the novel agonist 5-iodo-A-85380. *Neuropharmacol*. 2004;47:848–859.
- Kulak JM, Sum J, Musachio JL, McIntosh JM, Quik M. 5-Iodo-A-85380 binds to  $\alpha$ -conotoxin MII-sensitive nicotinic acetylcholine receptors (nAChRs) as well as  $\alpha_4\beta_2^*$  subtypes. *J Neurochem*. 2002;81:403–406.
- Kozikowski AP, Musachio JL, Kellar KJ, Xiao Y, Wei Z-L, inventors; Georgetown University, assignee. Ligands for nicotinic acetylcholine receptors, and methods of making and using them. WO 2005/000806. June 6, 2005.
- Zwart R, Carbone AL, Moroni M, et al. Sazetidine-A is a potent and selective agonist at native and recombinant  $\alpha_4\beta_2$  nicotinic acetylcholine receptors. *Mol Pharmacol*. 2008;73:1838–1843.
- Sullivan JP, Donnelly-Roberts DL, Briggs CA, et al. A-85830 [3-(2(S)-azetidylmethoxy)pyridine]: in vitro pharmacological properties of a novel high affinity  $\alpha_4\beta_2$  nicotinic acetylcholine receptor ligand. *Neuropharmacol*. 1996;35:725–734.
- Chattopadhyay S, Xue B, Collins D, et al. Synthesis and evaluation of nicotine  $\alpha_4\beta_2$  receptor radioligand, 5-(3'-( $^{18}\text{F}$ -fluoropropyl)-3-(2-(S)-pyrrolidinylmethoxy)pyridine, in rodents and PET in nonhuman primate. *J Nucl Med*. 2005;46:130–140.
- Xiao Y, Baydyuk M, Wang HP, Davis HE, Kellar KJ. Pharmacology of the agonist binding sites of rat neuronal nicotinic receptor subtypes expressed in HEK 293 cells. *Bioorg Med Chem Lett*. 2004;14:1845–1848.
- Logan J, Fowler JS, Volkow ND, et al. Graphical analysis of reversible radioligand binding from time-activity measurements applied to [ $^{11}\text{C}$ -methyl]-(-)-cocaine PET studies in human subjects. *J Cereb Blood Flow Metab*. 1990;10:740–747.
- Quik M, Vailati S, Bordia T, et al. Subunit composition of nicotinic receptors in monkey striatum: effect of treatments with 1-methyl-4-phenyl-1,2,3,6-tetrahydropyridine or L-DOPA. *Mol Pharmacol*. 2005;67:32–41.